

Transverse spin-dependent azimuthal correlations of charged pion pairs measured in $p^\uparrow + p$ collisions at $\sqrt{s} = 500$ GeV

L. Adamczyk¹, J. R. Adams²⁹, J. K. Adkins¹⁹, G. Agakishiev¹⁷, M. M. Aggarwal³¹, Z. Ahammed⁵⁴, N. N. Ajitanand⁴², I. Alekseev^{15,26}, D. M. Anderson⁴⁴, R. Aoyama⁴⁸, A. Aparin¹⁷, D. Arkhipkin³, E. C. Aschenauer³, M. U. Ashraf⁴⁷, A. Attri³¹, G. S. Averichev¹⁷, V. Bairathi²⁷, K. Barish⁵⁰, A. Behera⁴², R. Bellwied⁴⁶, A. Bhasin¹⁶, A. K. Bhati³¹, P. Bhattarai⁴⁵, J. Bielcik¹⁰, J. Bielcikova¹¹, L. C. Bland³, I. G. Bordyuzhin¹⁵, J. Bouchet¹⁸, J. D. Brandenburg³⁶, A. V. Brandin²⁶, D. Brown²³, J. Bryslawskyj⁵⁰, I. Bunzarov¹⁷, J. Butterworth³⁶, H. Caines⁵⁸, M. Calderón de la Barca Sánchez⁵, J. M. Campbell²⁹, D. Cebra⁵, I. Chakaberia³, P. Chaloupka¹⁰, Z. Chang⁴⁴, N. Chankova-Bunzarova¹⁷, A. Chatterjee⁵⁴, S. Chattopadhyay⁵⁴, J. H. Chen⁴¹, X. Chen²¹, X. Chen³⁹, J. Cheng⁴⁷, M. Cherney⁹, W. Christie³, G. Contin²², H. J. Crawford⁴, T. G. Dedovich¹⁷, J. Deng⁴⁰, I. M. Deppner⁵¹, A. A. Derevschikov³³, L. Didenko³, C. Dilks³², X. Dong²², J. L. Drachenberg²⁰, J. E. Draper⁵, J. C. Dunlop³, L. G. Efimov¹⁷, N. Elsey⁵⁶, J. Engelage⁴, G. Eppley³⁶, R. Esha⁶, S. Esumi⁴⁸, O. Evdokimov⁸, J. Ewigleben²³, O. Eyser³, R. Fatemi¹⁹, S. Fazio³, P. Federic¹¹, P. Federicova¹⁰, J. Fedorisin¹⁷, Z. Feng⁷, P. Filip¹⁷, E. Finch⁴⁹, Y. Fisyak³, C. E. Flores⁵, J. Fujita⁹, L. Fulek¹, C. A. Gagliardi⁴⁴, F. Geurts³⁶, A. Gibson⁵³, M. Girard⁵⁵, D. Grosnick⁵³, D. S. Gunarathne⁴³, Y. Guo¹⁸, A. Gupta¹⁶, W. Guryn³, A. I. Hamad¹⁸, A. Hamed⁴⁴, A. Harlanderova¹⁰, J. W. Harris⁵⁸, L. He³⁴, S. Heppelmann⁵, S. Heppelmann³², N. Herrmann⁵¹, A. Hirsch³⁴, S. Horvat⁵⁸, X. Huang⁴⁷, H. Z. Huang⁶, T. Huang²⁸, B. Huang⁸, T. J. Humanic²⁹, P. Huo⁴², G. Igo⁶, W. W. Jacobs¹⁴, A. Jentsch⁴⁵, J. Jia^{3,42}, K. Jiang³⁹, S. Jowzaee⁵⁶, E. G. Judd⁴, S. Kabana¹⁸, D. Kalinkin¹⁴, K. Kang⁴⁷, D. Kapukchyan⁵⁰, K. Kauder⁵⁶, H. W. Ke³, D. Keane¹⁸, A. Kechechyan¹⁷, Z. Khan⁸, D. P. Kikola⁵⁵, C. Kim⁵⁰, I. Kisel¹², A. Kisiel⁵⁵, L. Kochenda²⁶, M. Kocmanek¹¹, T. Kollegger¹², L. K. Kosarzewski⁵⁵, A. F. Kraishan⁴³, L. Krauth⁵⁰, P. Kravtsov²⁶, K. Krueger², N. Kulathunga⁴⁶, L. Kumar³¹, J. Kvapil¹⁰, J. H. Kwasizur¹⁴, R. Lacey⁴², J. M. Landgraf³, K. D. Landry⁶, J. Lauret³, A. Lebedev³, R. Lednický¹⁷, J. H. Lee³, W. Li⁴¹, C. Li³⁹, X. Li³⁹, Y. Li⁴⁷, J. Lidrych¹⁰, T. Lin¹⁴, M. A. Lisa²⁹, Y. Liu⁴⁴, H. Liu¹⁴, F. Liu⁷, P. Liu⁴², T. Ljubicic³, W. J. Llope⁵⁶, M. Lomnitz²², R. S. Longacre³, X. Luo⁷, S. Luo⁸, L. Ma⁴¹, Y. G. Ma⁴¹, G. L. Ma⁴¹, R. Ma³, N. Magdy⁴², R. Majka⁵⁸, D. Mallick²⁷, S. Margetis¹⁸, C. Markert⁴⁵, H. S. Matis²², D. Mayes⁵⁰, K. Meehan⁵, J. C. Mei⁴⁰, Z. W. Miller⁸, N. G. Minaev³³, S. Mioduszewski⁴⁴, D. Mishra²⁷, S. Mizuno²², B. Mohanty²⁷, M. M. Mondal¹³, D. A. Morozov³³, M. K. Mustafa²², Md. Nasim⁶, T. K. Nayak⁵⁴, J. M. Nelson⁴, D. B. Nemes⁵⁸, M. Nie⁴¹, G. Nigmatkulov²⁶, T. Niida⁵⁶, L. V. Nogach³³, T. Nonaka⁴⁸, S. B. Nurushev³³, G. Odyniec²², A. Ogawa³, K. Oh³⁵, V. A. Okorokov²⁶, D. Olivitt Jr.⁴³, B. S. Page³, R. Pak³, Y. Pandit⁸, Y. Panebratsev¹⁷, B. Pawlik³⁰, H. Pei⁷, C. Perkins⁴, J. Pluta⁵⁵, K. Poniatowska⁵⁵, J. Porter²², M. Posik⁴³, N. K. Pruthi³¹, M. Przybycien¹, J. Putschke⁵⁶, A. Quintero⁴³, S. Ramachandran¹⁹, R. L. Ray⁴⁵, R. Reed²³, M. J. Rehbein⁹, H. G. Ritter²², J. B. Roberts³⁶, O. V. Rogachevskiy¹⁷, J. L. Romero⁵, J. D. Roth⁹, L. Ruan³, J. Rusnak¹¹, O. Rusnakova¹⁰, N. R. Sahoo⁴⁴, P. K. Sahu¹³, S. Salur³⁷, J. Sandweiss⁵⁸, M. Saur¹¹, J. Schambach⁴⁵, A. M. Schmah²², W. B. Schmidke³, N. Schmitz²⁴, B. R. Schweid⁴², J. Seger⁹, M. Sergeeva⁶, R. Seto⁵⁰, P. Seyboth²⁴, N. Shah⁴¹, E. Shahaliev¹⁷, P. V. Shanmuganathan²³, M. Shao³⁹, W. Q. Shen⁴¹, S. S. Shi⁷, Z. Shi²², Q. Y. Shou⁴¹, E. P. Sichtermann²², R. Sikora¹, M. Simko¹¹, S. Singha¹⁸, M. J. Skoby¹⁴, N. Smirnov⁵⁸, D. Smirnov³, W. Solyst¹⁴, P. Sorensen³, H. M. Spinka², B. Srivastava³⁴, T. D. S. Stanislaus⁵³, D. J. Stewart⁵⁸, M. Strikhanov²⁶, B. Stringfellow³⁴, A. A. P. Suaide³⁸, T. Sugiura⁴⁸, M. Sumera¹¹, B. Summa³², X. Sun⁷, X. M. Sun⁷, Y. Sun³⁹, B. Surrow⁴³, D. N. Svirida¹⁵, Z. Tang³⁹, A. H. Tang³, A. Taranenko²⁶, T. Tarnowsky²⁵, A. Tawfik⁵⁷, J. Thäder²², J. H. Thomas²², A. R. Timmins⁴⁶, D. Tlusty³⁶, T. Todoroki³, M. Tokarev¹⁷, S. Trentalange⁶, R. E. Tribble⁴⁴, P. Tribedy³, S. K. Tripathy¹³, B. A. Trzeciak¹⁰, O. D. Tsai⁶, B. Tu⁷, T. Ullrich³, D. G. Underwood², I. Upsal²⁹, G. Van Buren³, G. van Nieuwenhuizen³, A. N. Vasiliev³³, F. Videbæk³, S. Vokal¹⁷, S. A. Voloshin⁵⁶, A. Vossen¹⁴, G. Wang⁶, Y. Wang⁴⁷, Y. Wang⁷, F. Wang³⁴, G. Webb³, J. C. Webb³, L. Wen⁶, G. D. Westfall²⁵, H. Wieman²², S. W. Wissink¹⁴, R. Witt⁵², Y. Wu¹⁸, Z. G. Xiao⁴⁷, G. Xie³⁹, W. Xie³⁴, N. Xu²², Y. F. Xu⁴¹, Q. H. Xu⁴⁰, Z. Xu³, Y. Yang²⁸, C. Yang⁴⁰, S. Yang³, Q. Yang⁴⁰, Z. Ye⁸, Z. Ye⁸, L. Yi⁵⁸, K. Yip³, I. -K. Yoo³⁵, H. Zbroszczyk⁵⁵, W. Zha³⁹, J. B. Zhang⁷, J. Zhang²², S. Zhang³⁹, J. Zhang²¹, S. Zhang⁴¹, Z. Zhang⁴¹, Y. Zhang³⁹, L. Zhang⁷,

X. P. Zhang⁴⁷, J. Zhao³⁴, C. Zhong⁴¹, C. Zhou⁴¹, L. Zhou³⁹, X. Zhu⁴⁷, Z. Zhu⁴⁰, M. Zyzak¹²

- ¹*AGH University of Science and Technology, FPACS, Cracow 30-059, Poland*
- ²*Argonne National Laboratory, Argonne, Illinois 60439*
- ³*Brookhaven National Laboratory, Upton, New York 11973*
- ⁴*University of California, Berkeley, California 94720*
- ⁵*University of California, Davis, California 95616*
- ⁶*University of California, Los Angeles, California 90095*
- ⁷*Central China Normal University, Wuhan, Hubei 430079*
- ⁸*University of Illinois at Chicago, Chicago, Illinois 60607*
- ⁹*Creighton University, Omaha, Nebraska 68178*
- ¹⁰*Czech Technical University in Prague, FNSPE, Prague, 115 19, Czech Republic*
- ¹¹*Nuclear Physics Institute AS CR, 250 68 Prague, Czech Republic*
- ¹²*Frankfurt Institute for Advanced Studies FIAS, Frankfurt 60438, Germany*
- ¹³*Institute of Physics, Bhubaneswar 751005, India*
- ¹⁴*Indiana University, Bloomington, Indiana 47408*
- ¹⁵*Alikhanov Institute for Theoretical and Experimental Physics, Moscow 117218, Russia*
- ¹⁶*University of Jammu, Jammu 180001, India*
- ¹⁷*Joint Institute for Nuclear Research, Dubna, 141 980, Russia*
- ¹⁸*Kent State University, Kent, Ohio 44242*
- ¹⁹*University of Kentucky, Lexington, Kentucky 40506-0055*
- ²⁰*Lamar University, Physics Department, Beaumont, Texas 77710*
- ²¹*Institute of Modern Physics, Chinese Academy of Sciences, Lanzhou, Gansu 730000*
- ²²*Lawrence Berkeley National Laboratory, Berkeley, California 94720*
- ²³*Lehigh University, Bethlehem, Pennsylvania 18015*
- ²⁴*Max-Planck-Institut für Physik, Munich 80805, Germany*
- ²⁵*Michigan State University, East Lansing, Michigan 48824*
- ²⁶*National Research Nuclear University MEPhI, Moscow 115409, Russia*
- ²⁷*National Institute of Science Education and Research, HBNI, Jatni 752050, India*
- ²⁸*National Cheng Kung University, Tainan 70101*
- ²⁹*Ohio State University, Columbus, Ohio 43210*
- ³⁰*Institute of Nuclear Physics PAN, Cracow 31-342, Poland*
- ³¹*Panjab University, Chandigarh 160014, India*
- ³²*Pennsylvania State University, University Park, Pennsylvania 16802*
- ³³*Institute of High Energy Physics, Protvino 142281, Russia*
- ³⁴*Purdue University, West Lafayette, Indiana 47907*
- ³⁵*Pusan National University, Pusan 46241, Korea*
- ³⁶*Rice University, Houston, Texas 77251*
- ³⁷*Rutgers University, Piscataway, New Jersey 08854*
- ³⁸*Universidade de Sao Paulo, Sao Paulo, Brazil, 05314-970*
- ³⁹*University of Science and Technology of China, Hefei, Anhui 230026*

- ⁴⁰Shandong University, Jinan, Shandong 250100
- ⁴¹Shanghai Institute of Applied Physics, Chinese Academy of Sciences, Shanghai 201800
- ⁴²State University of New York, Stony Brook, New York 11794
- ⁴³Temple University, Philadelphia, Pennsylvania 19122
- ⁴⁴Texas A&M University, College Station, Texas 77843
- ⁴⁵University of Texas, Austin, Texas 78712
- ⁴⁶University of Houston, Houston, Texas 77204
- ⁴⁷Tsinghua University, Beijing 100084
- ⁴⁸University of Tsukuba, Tsukuba, Ibaraki, Japan, 305-8571
- ⁴⁹Southern Connecticut State University, New Haven, Connecticut 06515
- ⁵⁰University of California, Riverside, California 92521
- ⁵¹University of Heidelberg
- ⁵²United States Naval Academy, Annapolis, Maryland 21402
- ⁵³Valparaiso University, Valparaiso, Indiana 46383
- ⁵⁴Variable Energy Cyclotron Centre, Kolkata 700064, India
- ⁵⁵Warsaw University of Technology, Warsaw 00-661, Poland
- ⁵⁶Wayne State University, Detroit, Michigan 48201
- ⁵⁷World Laboratory for Cosmology and Particle Physics (WLCAPP), Cairo 11571, Egypt
- ⁵⁸Yale University, New Haven, Connecticut 06520

Abstract

The transversity distribution, which describes transversely polarized quarks in transversely polarized nucleons, is a fundamental component of the spin structure of the nucleon, and is only loosely constrained by global fits to existing semi-inclusive deep inelastic scattering (SIDIS) data. In transversely polarized $p^\uparrow + p$ collisions it can be accessed using transverse polarization dependent fragmentation functions which give rise to azimuthal correlations between the polarization of the struck parton and the final state scalar mesons.

This letter reports on spin dependent di-hadron correlations measured by the STAR experiment. The new dataset corresponds to 25 pb^{-1} integrated luminosity of $p^\uparrow + p$ collisions at $\sqrt{s} = 500 \text{ GeV}$, an increase of more than a factor of ten compared to our previous measurement at $\sqrt{s} = 200 \text{ GeV}$. Non-zero asymmetries sensitive to transversity are observed at a Q^2 of several hundred GeV and are found to be consistent with the former measurement and a model calculation. We expect that these data will enable an extraction of transversity with comparable precision to current SIDIS datasets but at much higher momentum transfers where subleading effects are suppressed.

Keywords: transversity, di-hadron correlations, interference fragmentation function

1. Introduction

The proton is the fundamental bound state of quantum chromodynamics (QCD). In spite of its importance for our understanding of this theory, our knowledge of the proton structure remains incomplete [1]. In particular, the proton wave function cannot be computed ab-initio in perturbative QCD (pQCD), but has to be constrained by measurements. In deep inelastic scattering (DIS) experiments of electrons or muons off nuclei at high energies, the wavefunction of the proton is accessed on the lightcone. In this frame, the wavefunction can be expanded in the squared 4-momentum transfer Q^2 of the interaction. The leading coefficients in this expansion can be identified with three parton distribution functions (PDFs). In the parton model, PDFs have a probabilistic interpretation as the probability of finding a parton that carries a momentum fraction x of the parent proton. The moderate Q^2 dependence, which arises from the parton splitting functions [2, 3, 4], is computed using evolution equations. We assume a Q^2 dependence in the following discussion even when not explicitly written. Two of the PDFs, the parton helicity averaged PDF $f_1(x)$, and the helicity PDF $g_1(x)$ appear at leading twist respectively in the spin averaged and longitudinally polarized inclusive DIS cross-section [5]. They are therefore fairly well determined experimentally [6]. The third one, the transversity distribution $h_1(x)$, does not appear at leading twist in the inclusive DIS cross-section since it is connected to a chiral-odd helicity-flip amplitude. Instead, it is accessed in processes where it couples to the chiral-odd transverse spin dependent fragmentation function (FF) [7]. The transversity PDF can be interpreted as the probability of finding a transversely polarized quark in a transversely polarized proton, and the FF serves as a quark polarimeter.

The analysis presented here investigates a channel in which transversity couples to the spin dependent di-hadron FF $H_1^\zeta(z, M)$ [8, 9, 10], which, for historical reasons, is also known as the interference fragmentation function (IFF). Here, z is the fraction of the parent parton energy carried by the hadron pair, and M is the invariant mass of the pair. Presently, transversity is only loosely constrained by fits [11, 12] to available SIDIS [13, 14, 15, 16, 17] and e^+e^- [18, 19] data. The e^+e^- data are necessary to constrain the polarization dependent fragmentation functions. Data on proton targets are currently limited in the valence region to $x < 0.2$, restricting the knowledge of u quark transversity at high x . Probing transversity in $p+p$ collisions provides better access to the d -quark transversity than is possible in SIDIS, due to the fact that there is no charge weighting in the hard scattering QCD $2 \rightarrow 2$ processes in $p+p$ collisions. A precision determination of both u and d -quark transversity are important in particular for the determination of the zeroth moment of transversity, the tensor charge

$$g_T = \int_0^1 dx [h_1^q(x) - h_1^{\bar{q}}(x)] \quad (1)$$

Recently, g_T has attracted increased interest. One reason is that it can be calculated precisely using lattice QCD [20, 21, 22, 23, 24], which makes it one of the few observables involving transverse polarization where experiments can be compared with first order pQCD calculations. In fact, g_T is the first nucleon

matrix element that could be extrapolated to the physical limit. Furthermore, g_T determines the effective tensor coupling constant for beyond the standard model contributions to low energy scattering [25]. This determination is particularly important for planned electric dipole moment experiments where a precise knowledge of g_T is needed to determine the contributions of possible new CP violating phases [26]. Due to its chiral-odd property, gluon polarization contributions to transversity in a spin- $\frac{1}{2}$ target vanish [27]. This characteristic is one reason g_T is dominated by medium to high x region. Precision data from transversely polarized $p + p$ collisions at high \sqrt{s} and p_T are crucial to access transversity at high Q^2 , where theoretical uncertainties are well under control. The kinematic region covered by the STAR experiment at these energies overlaps the reach of current SIDIS experimental data on transversity in the upper part of the covered x range (see Fig. 1). The STAR kinematics is obtained from the transverse momentum of the mid-rapidity jet containing the hadron pair since this is the relevant scale in $p + p$ collision and approximately equal to Q^2 . The results presented in this letter at $\sqrt{s} = 500$ GeV use more than 10 times the integrated luminosity than our previously reported result at $\sqrt{s} = 200$ GeV [28], where a significant signal of transversity was observed in an exploratory measurement of di-pion correlations [28]. The calculations reported in [12] found hints of universality where the phase space of the $\sqrt{s} = 200$ GeV $p + p$ and the SIDIS data overlap. Since the calculations are performed in a collinear framework, this was already postulated. However, since factorization is not proven in this process and has been explicitly shown to be broken in other transverse polarization dependent processes in $p + p$ [29], this was a crucial finding to support the inclusion of the data in global analyses. In the future, a comparison between di-hadron asymmetries, with measurements of azimuthal asymmetries of pions in jets by STAR [30], will provide further tests of universality and factorization. The former asymmetries can be described in a collinear framework, while the latter include an explicit dependency on intrinsic transverse momenta (for more details see [31, 32]). The collinear framework is well understood and describes the unpolarized $p + p$ cross-section well [33], but the transverse momentum dependent (TMD) framework is still being developed, and questions remain about universality, factorization and evolution.

2. Experiment

The Relativistic Heavy Ion Collider (RHIC), located at Brookhaven National Laboratory, can collide beams of polarized protons, as well as heavy ions, at each of the interaction regions. The data used in this analysis were recorded at the STAR experiment in 2011 representing 25 pb $^{-1}$ integrated luminosity of transversely polarized $p + p$ collisions at $\sqrt{s} = 500$ GeV and an average beam polarization of 53%. Kinematic observables of charged particles are measured using the Time Projection Chamber (TPC) with 2π azimuthal coverage in the pseudorapidity range $-1 \lesssim \eta \lesssim 1$ [34]. The barrel and endcap electromagnetic calorimeters (BEMC/EEMC) and the beam-beam counters (BBC) are used in coincidence for the trigger. A single BEMC tower is required to have a minimum transverse energy ($E_T > 4.0$ or 5.7 GeV) or a $\Delta\phi \times \Delta\eta = 1.0 \times 1.0$ jet

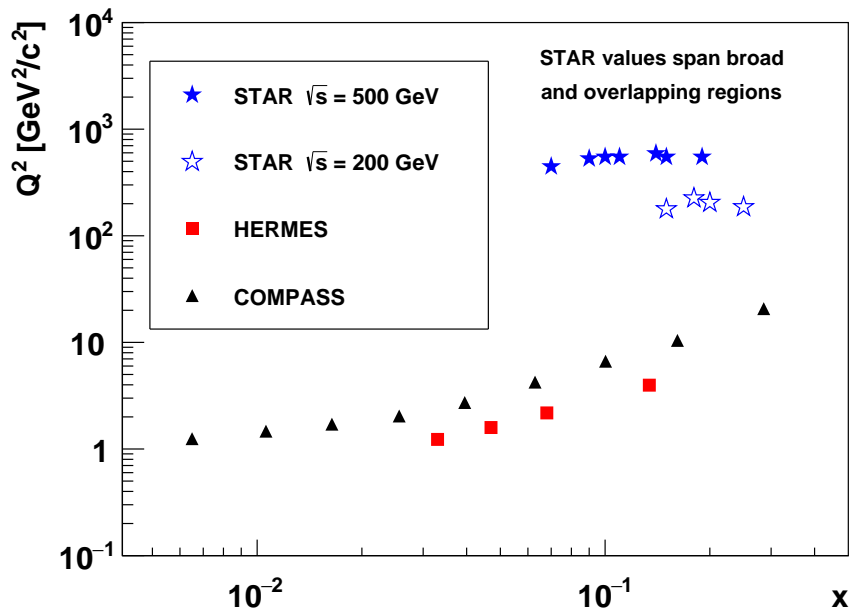


Figure 1: Q^2 vs x coverage for STAR, HERMES, and COMPASS [13, 14, 15, 16, 17]. The kinematics of the STAR data points correspond to the lower panel of Fig. 3.

patch must have $E_T > 6.4, 9.0$ or 13.9 GeV, respectively. Particles are identified by measuring their average specific ionization energy loss, $\langle dE/dx \rangle$, as they traverse the TPC and comparing this measured value with the associated parameterized expectation for each particle species as a function of η and momentum. Cuts on the number of standard deviations from the pion $\langle dE/dx \rangle$ peak (-1σ to 2σ) and the number of hits used to determine $\langle dE/dx \rangle$ (> 20) are applied to achieve an $85 \pm 2.5\%$ pion pair purity across the entire kinematic range. The pion pair purity is the probability that both particles in a pair are pions. The momentum, p , of each particle is required to be greater than 2 GeV/ c .

Each proton beam in the RHIC ring consists of bunches that alternate between being transversely polarized up or down with respect to the accelerator plane. However, when the single spin asymmetry measurement is carried out with respect to a given beam, the polarization of the other beam is integrated over to effectively be unpolarized. Polarimeters, which measure the elastic scattering of protons on ultra thin carbon ribbon targets several times during a fill, were used to measure the polarization of each beam. These polarimeters were calibrated with a polarized hydrogen gas jet target [35].

3. Analysis

The azimuthal angles in the scattering system used to calculate the $\pi^+\pi^-$ azimuthal correlation follow the definition in ref. [37] and are shown in Fig. 2. The scattering plane is defined by the polarized beam direction, \vec{p}_{beam} , and the direction of the total momentum of the pion pair, \vec{p}_h . The di-hadron plane is defined

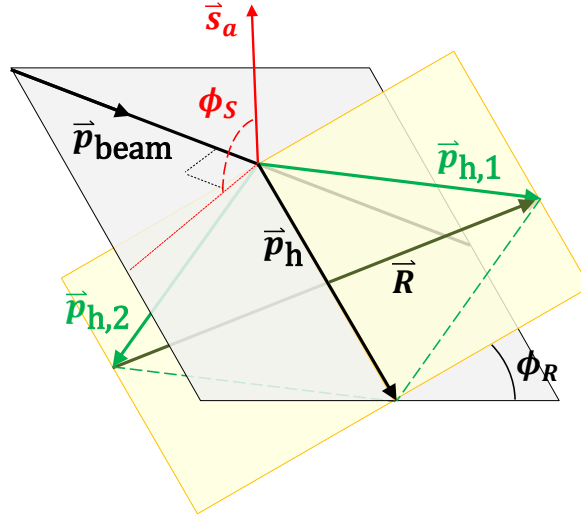


Figure 2: Diagram of the azimuthal angle, where $\vec{p}_{h,1(2)}$ is the momentum of the positive (negative) pion, \vec{s}_a is the beam polarization, and ϕ_R is the angle between the scattering plane (blue) and the di-hadron plane (yellow).

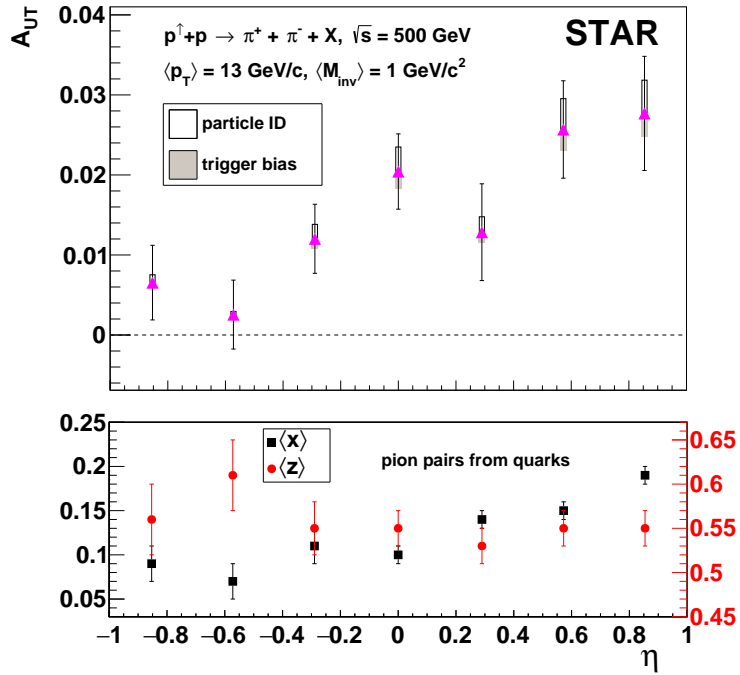


Figure 3: A_{UT} (top) and the kinematic variables, $\langle x \rangle$ and $\langle z \rangle$ (bottom), plotted as a function of η for pairs that arise from quarks. Statistical uncertainties are represented by the error bars, the open rectangles are the systematic uncertainties originating from the particle identification, and the solid rectangles represent the trigger bias systematic uncertainties.

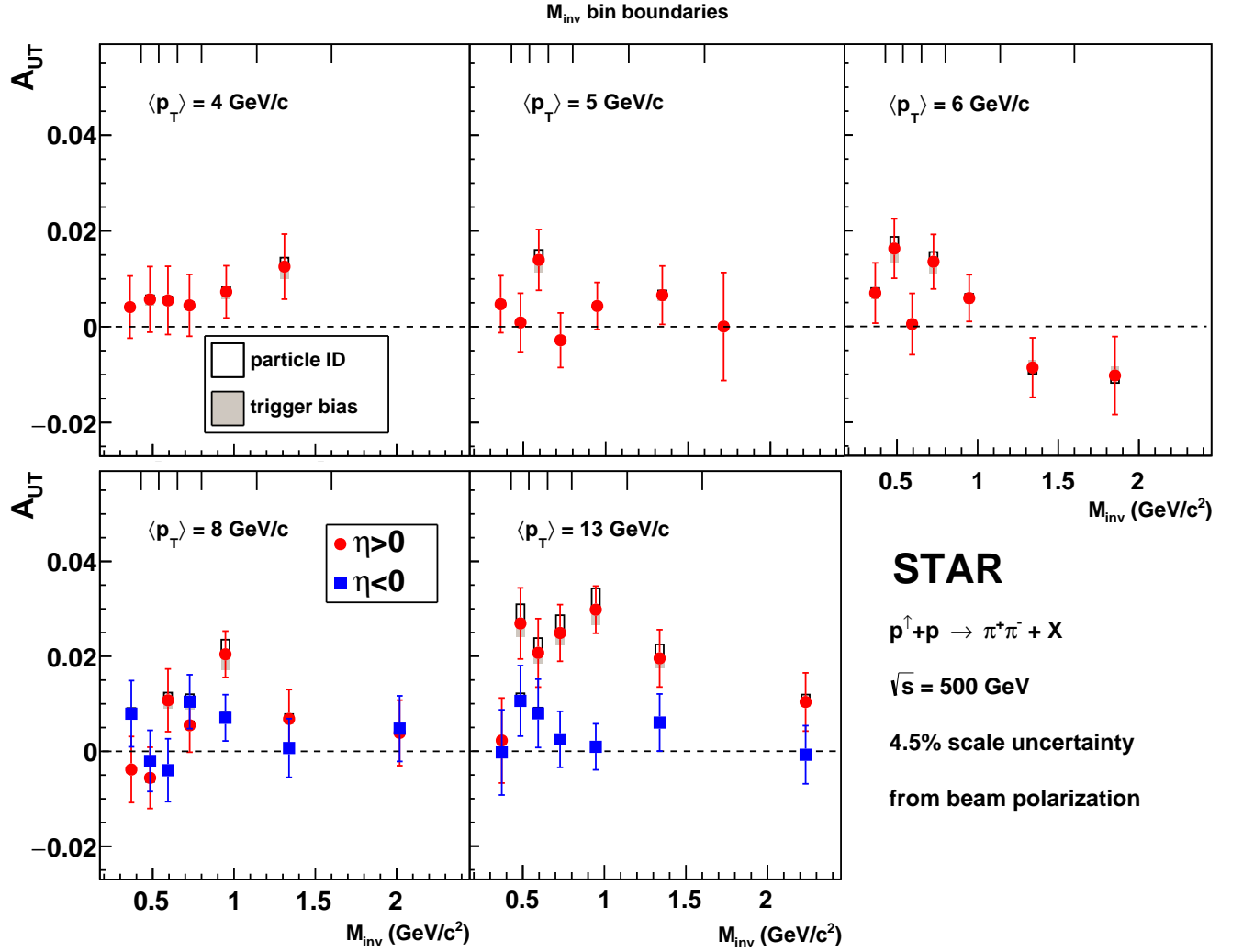


Figure 4: The asymmetry A_{UT} as a function of M_{inv} for five p_T bins. Statistical uncertainties are represented by the error bars, the open rectangles are the systematic uncertainties originating from the particle identification, and the solid one represent the trigger bias systematic uncertainties. The M_{inv} bin boundaries are shown at the top of each panel.

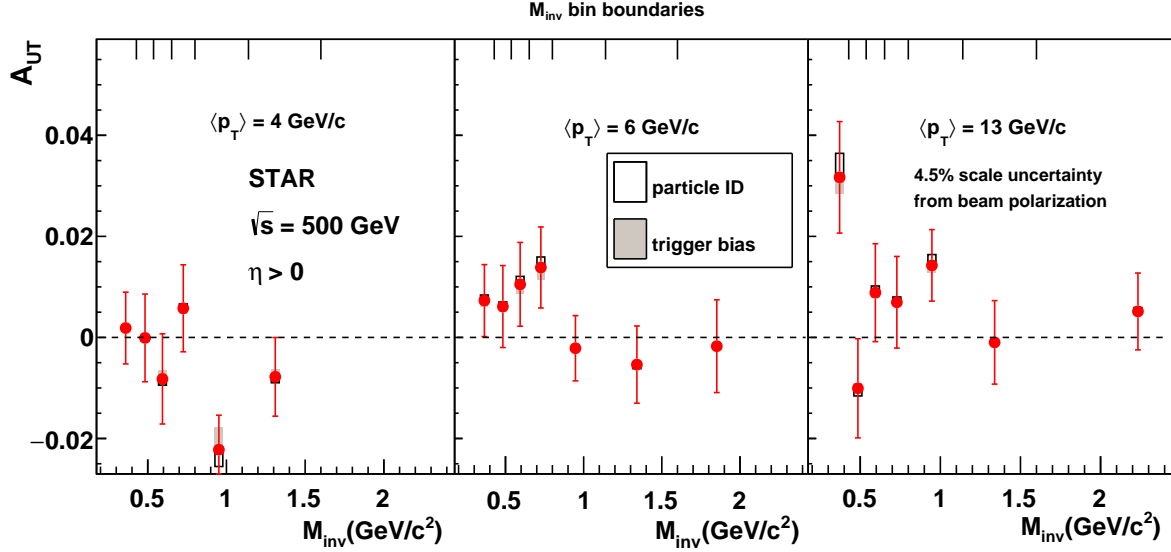


Figure 5: The same-charge, momentum-ordered ($|\vec{p}_{h,1}| > |\vec{p}_{h,2}|$) asymmetry A_{UT} as a function of M_{inv} for the lowest p_T bin, mid- p_T bin, and the highest p_T bin used in Fig. 4. Statistical uncertainties are represented by the error bars, the open rectangles are the systematic uncertainties originating from the particle identification, and the solid one represent the trigger bias systematic uncertainties. The M_{inv} bin boundaries are shown at the top of the figure.

by the momentum vectors from each pion ($\vec{p}_{h,1}$ and $\vec{p}_{h,2}$) in the pair. The difference vector $\vec{R} = \vec{p}_{h,1} - \vec{p}_{h,2}$ lies in the di-hadron plane. The pions are chosen to be in close proximity to each other in $\eta - \phi$ space with $\sqrt{(\Delta\eta)^2 + (\Delta\phi)^2} \leq 0.7$ and the sum of the transverse momenta, p_T , for each pair is required to be greater than $3.75 \text{ GeV}/c$. Throughout the rest of this paper, p_T is the transverse momentum of the pion pair and $\vec{p}_{h,1}$ corresponds to the positive pion and $\vec{p}_{h,2}$ to the negative pion. We define the unit vectors $\hat{p} = \vec{p}/|\vec{p}|$. The angle between the scattering plane and the polarization of the incident beam, \vec{s}_a , is ϕ_S . The angle between the scattering plane and the di-hadron plane is ϕ_R , which is used to define $\phi_{RS} = \phi_R - \phi_S$, where ϕ_R and ϕ_S are calculated using Eqs. (2)–(5). The angle ϕ_{RS} modulates the asymmetry due to the product of transversity and the IFF by $\sin(\phi_{RS})$.

$$\cos(\phi_S) = \frac{\hat{p}_{beam} \times \vec{p}_h}{|\hat{p}_{beam} \times \vec{p}_h|} \cdot \frac{\hat{p}_{beam} \times \vec{s}_a}{|\hat{p}_{beam} \times \vec{s}_a|} \quad (2)$$

$$\sin(\phi_S) = \frac{(\vec{p}_h \times \vec{s}_a) \cdot \hat{p}_{beam}}{|\hat{p}_{beam} \times \vec{p}_h| |\hat{p}_{beam} \times \vec{s}_a|} \quad (3)$$

$$\cos(\phi_R) = \frac{\hat{p}_h \times \vec{p}_{beam}}{|\hat{p}_h \times \vec{p}_{beam}|} \cdot \frac{\hat{p}_h \times \vec{R}}{|\hat{p}_h \times \vec{R}|} \quad (4)$$

$$\sin(\phi_R) = \frac{(\vec{p}_{beam} \times \vec{R}) \cdot \hat{p}_h}{|\hat{p}_h \times \vec{p}_{beam}| |\hat{p}_h \times \vec{R}|} \quad (5)$$

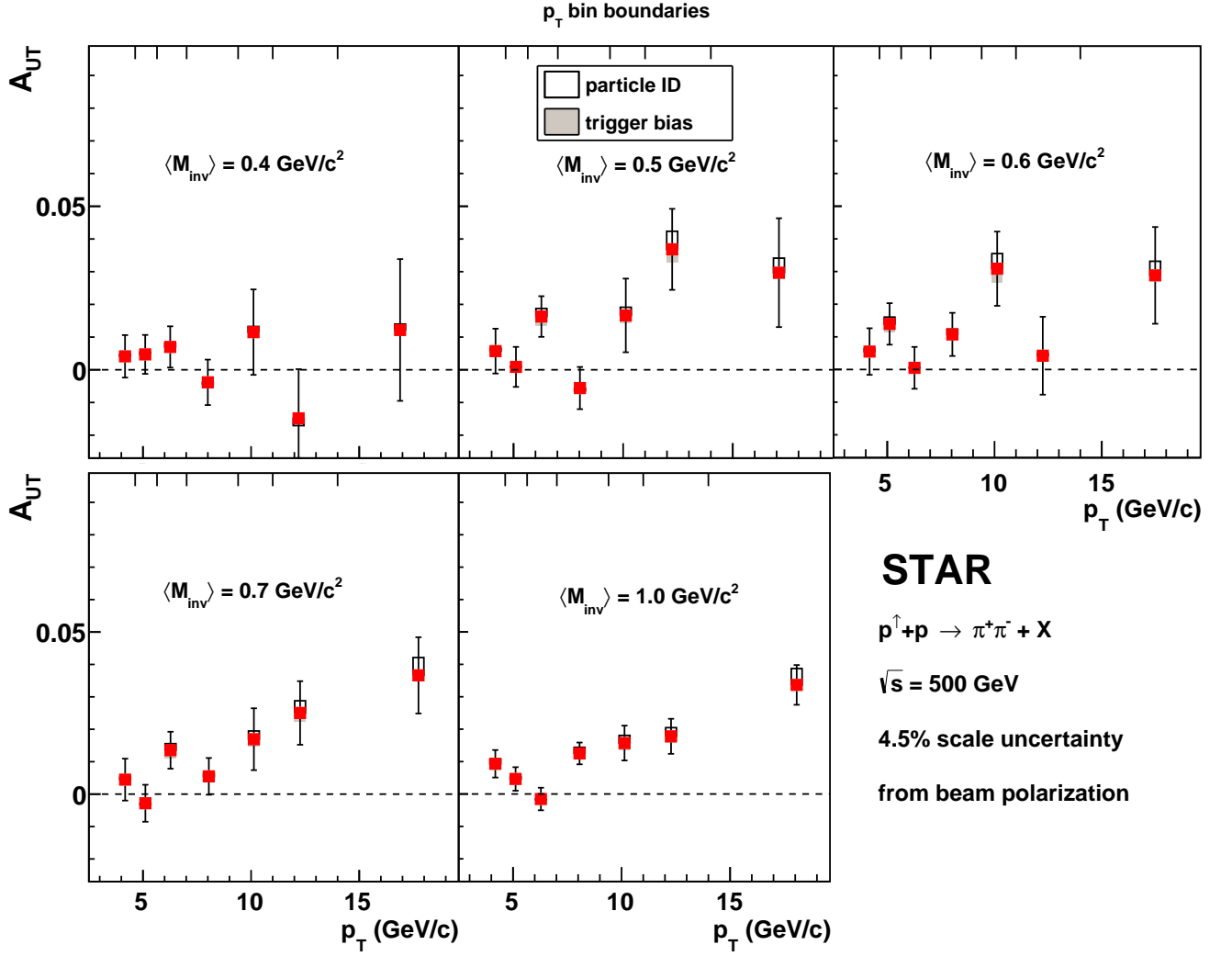


Figure 6: The asymmetry A_{UT} as a function of p_T for five M_{inv} bins. Statistical uncertainties are represented by the error bars, the open rectangles are the systematic uncertainties originating from the particle identification, and the solid one represent the trigger bias systematic uncertainties. The p_T bin boundaries are shown at the top of the figure.

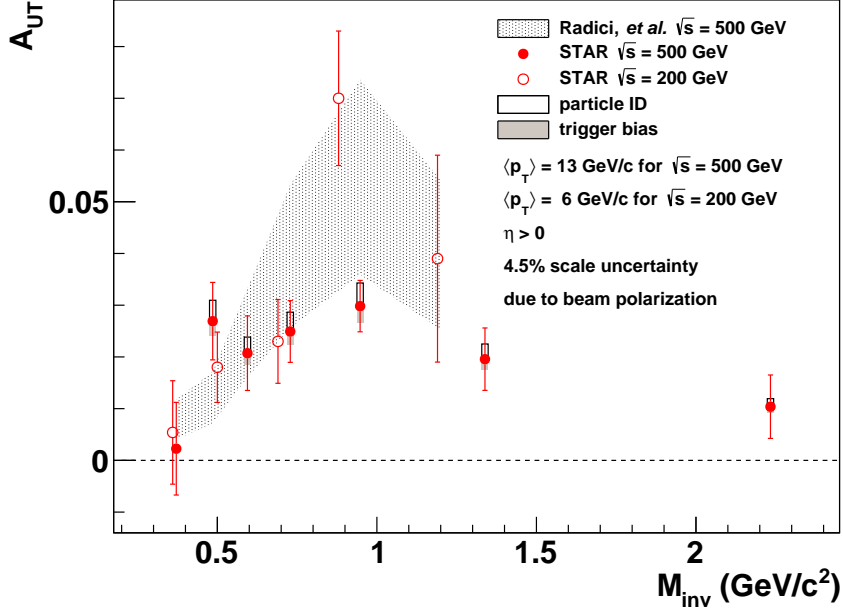


Figure 7: The azimuthal asymmetry as a function of invariant mass in the highest p_T bin compared with predictions from fits to existing SIDIS and e^+e^- data provided by the same authors as [12]. Details on the calculation can be found in [36].

The $\pi^+\pi^-$ azimuthal correlation observable, A_{UT} , is defined in Eq. (6), where P is the beam polarization and $N^{\uparrow(\downarrow)}$ is the number of pion pairs when the polarization of the beam is pointing up (down). The combination of different polarization directions and detector hemispheres removes luminosity and efficiency dependencies from the asymmetry calculation to leading order [38].

A_{UT} is calculated for eight ϕ_{RS} bins of equal width in the range $[0, \pi]$, which are then fitted with a single-parameter function, $A_{UT} \cdot \sin(\phi_{RS})$, to extract the amplitude. This procedure is carried out as a function of the pseudorapidity of the pion pair, which is denoted as η for the remainder of this report. $\eta > 0$ is forward with respect to the polarized beam direction. A_{UT} is also measured as a function of invariant mass, M_{inv} , and p_T .

$$A_{UT} \cdot P \cdot \sin(\phi_{RS}) = \frac{\sqrt{N^{\uparrow}(\phi_{RS})N^{\downarrow}(\phi_{RS} + \pi)} - \sqrt{N^{\downarrow}(\phi_{RS})N^{\uparrow}(\phi_{RS} + \pi)}}{\sqrt{N^{\uparrow}(\phi_{RS})N^{\downarrow}(\phi_{RS} + \pi)} + \sqrt{N^{\downarrow}(\phi_{RS})N^{\uparrow}(\phi_{RS} + \pi)}}. \quad (6)$$

The scale uncertainty due to the beam polarization in this analysis is 4.5%. We investigated a potential bias of the triggered events towards pions that come from quark jets, which could result in an enhancement of the measured asymmetries, since gluons are not expected to contribute to transversity. To investigate this bias, particles produced in $p+p$ simulated events from PYTHIA 6.426 [39] with the Perugia-0 tune [40], were processed through a detector simulator (GSTAR package based upon GEANT 3.21/08T [41]), and then used to estimate the quark/parton ratio of a biased sample over the quark/parton ratio in an unbiased sample.

In STAR the trigger decision is based on the energy deposit in a defined segment in one of the calorimeters. We expect therefore that a potential trigger bias effect will be strongest for low p_T parent jets, since at high jet p_T the impact of a shape difference between quark or gluon initiated jets will be negligible for the trigger decision. For this reason we investigated the trigger bias as a function of the transverse momentum of the hadron pair. Within our statistical uncertainties, we do not observe a significant trigger bias and thus decided not to correct for this effect. Instead, the statistical uncertainty with which one can determine the ratio of the fractions of quark initiated jets in the triggered over the non-triggered sample was assigned as a systematic uncertainty, being $\sim 20\%$ at low p_T and $\sim 5\%$ at high p_T . Note that the trigger bias does not affect the statistical significance of the measurement because the scaling applies to the asymmetry and its uncertainty equally. Since the trigger efficiency is higher for larger jet energies, the selection of pion pairs might be biased towards lower z pairs. Using the same simulation as for the trigger bias, we estimate this effect to be $\sim 8\%$ at low p_T and $\sim 4\%$ at high p_T .

Finally, the pion pair purity previously mentioned was used to estimate the asymmetric asymmetry dilution due to $\pi - K$ and $\pi - p$ pairs and found to be about 15% and is represented as rectangles above (below) positive (negative) data points. This estimate assumes the $\pi - K$ and $\pi - p$ asymmetries are no larger than the $\pi^+ - \pi^-$ asymmetries and have the same sign.

4. Results

The single spin asymmetry, A_{UT} , was measured as a function of η for five p_T bins. It is shown as a function of η in Fig. 3 for the largest p_T bin with $\langle p_T \rangle = 13 \text{ GeV}/c$. The other four p_T bins have smaller asymmetries compared to the $\langle p_T \rangle$ bin in Fig. 3. Using the particles produced in PYTHIA and processed through GEANT as mentioned previously, the kinematic variables x and z were estimated. The bottom panel of Fig. 3 shows x and z as a function of pion pair pseudorapidity. As shown in Fig. 3, a strong rise of the measured signal is observed toward higher η where we reach the highest values of x . This is consistent with the expectation that the transversity distribution is largest at high- x .

A_{UT} as a function of M_{inv} for $\eta > 0$ is shown in Fig. 4 for the five p_T bins. Because A_{UT} is consistent across all p_T bins for $\eta < 0$ it is shown only for the two largest p_T bins. A significant signal is seen in the highest p_T bin, with an enhancement near the ρ mass at mid- M_{inv} . In models of the IFF, this enhancement is expected due to the interference of vector meson decays in a relative p -wave with the non-resonant background in a relative s -wave [9]. To test this hypothesis, the same-charge, momentum-ordered ($|\vec{p}_{h,1}| > |\vec{p}_{h,2}|$) asymmetry was calculated and is shown in Fig. 5. This plot shows a significantly smaller asymmetry around the ρ mass compared to the charge-ordered calculation. We note that this suppressed asymmetry can also be explained in single hadron emission models like the Nambu and Jona-Lasinio jet model [42] where the parton producing the lower ranked same-charge pion will carry less of

the spin information and is more likely to have a transverse momentum direction correlated (instead of anti-correlated) with the higher ranked pion.

A_{UT} as a function of p_T for $\eta > 0$ is shown in Fig. 6 for five M_{inv} bins. A significant asymmetry is observed at high p_T for $\langle M_{inv} \rangle > 0.4 \text{ GeV}/c^2$. Though not shown here, the asymmetry as a function of p_T for $\eta < 0$ is small compared to the results for $\eta > 0$. Supplemental tables containing the numerical results shown in the figures discussed above are available online.

Figure 7 shows a comparison of a theoretical calculation with the azimuthal asymmetry as a function of the invariant mass measured in $p^\dagger + p$ collisions at $\sqrt{s} = 500 \text{ GeV}$ for the highest p_T bin. The gray band represents the range of the 68% confidence interval of the fit to SIDIS and e^+e^- data. The fit has been provided by the authors of reference [12], which was first compared to the STAR results at $\sqrt{s} = 200 \text{ GeV}$ [28]. The smaller M_{inv} range for the theory band is due to the fact that this specific model calculation has only been performed up to $M_{inv} \approx 1.2 \text{ GeV}/c$. The asymmetry comparison shows close agreement within statistical uncertainty between the data and the theory band, which further hints at the universality of the mechanism producing azimuthal correlations in SIDIS, e^+e^- , and $p+p$ data. These high-precision $\sqrt{s} = 500 \text{ GeV}$ results can further constrain global fits of transversity parton distribution functions to SIDIS, e^+e^- , and $p+p$ data, and in particular, improve the statistical significance for $x > 0.1$.

5. Conclusions

STAR has measured the first $\pi^+\pi^-$ transverse spin-dependent azimuthal asymmetries in $p^\dagger + p$ collisions at $\sqrt{s} = 500 \text{ GeV}$ for several pseudorapidity, invariant mass, and transverse momentum bins. These data show significant signals at high p_T and M_{inv} for $\eta > 0$. IFF models predict an enhancement around the ρ mass due to the interference of vector meson decays in a relative p -wave with the non-resonant background in a relative s -wave. This prediction is consistent with the data reported in the paper. These data probe transversity at much higher $Q^2 \approx 400 \text{ GeV}^2$ and sample a different mixture of quark flavors compared to the charge weighted coupling in SIDIS. These results can be used to test the universality of the mechanism producing azimuthal correlations in SIDIS, e^+e^- , and $p+p$. In the future, a comparison between di-hadron asymmetries with measurements of azimuthal asymmetries of pions in jets will provide further tests of universality and factorization. Additionally, the high-precision of these results can further constrain global fits to world data, especially in the region $x > 0.1$.

6. Acknowledgements

We thank Marco Radici and Alessandro Bacchetta from the Department of Physics at the University of Pavia for helpful discussions and for providing theory curves for this work. We thank the RHIC Operations Group and RCF at BNL, the NERSC Center at LBNL, and the Open Science Grid consortium for providing

resources and support. This work was supported in part by the Office of Nuclear Physics within the U.S. DOE Office of Science, the U.S. National Science Foundation, the Ministry of Education and Science of the Russian Federation, National Natural Science Foundation of China, Chinese Academy of Science, the Ministry of Science and Technology of China and the Chinese Ministry of Education, the National Research Foundation of Korea, GA and MSMT of the Czech Republic, Department of Atomic Energy and Department of Science and Technology of the Government of India; the National Science Centre of Poland, National Research Foundation, the Ministry of Science, Education and Sports of the Republic of Croatia, RosAtom of Russia and German Bundesministerium für Bildung, Wissenschaft, Forschung und Technologie (BMBF) and the Helmholtz Association.

References

- [1] A. Aprahamian, et al., Reaching for the horizon: The 2015 long range plan for nuclear science.
- [2] G. Altarelli, G. Parisi, Asymptotic Freedom in Parton Language, Nucl. Phys. B126 (1977) 298–318. doi:10.1016/0550-3213(77)90384-4.
- [3] V. Gribov, L. Lipatov, Sov. J. Nucl. Phys. 15 (1972) 438.
- [4] Y. Dokshitzer, Sov.Phys. JETP 46 (1977) 641.
- [5] P. J. Mulders, R. D. Tangerman, The Complete tree level result up to order $1/Q$ for polarized deep inelastic lepton production, Nucl. Phys. B461 (1996) 197–237, [Erratum: Nucl. Phys.B484,538(1997)]. arXiv:hep-ph/9510301, doi:10.1016/S0550-3213(96)00648-7, 10.1016/0550-3213(95)00632-X.
- [6] C. A. Aidala, S. D. Bass, D. Hasch, G. K. Mallot, The Spin Structure of the Nucleon, Rev. Mod. Phys. 85 (2013) 655–691. arXiv:1209.2803, doi:10.1103/RevModPhys.85.655.
- [7] A. Metz, A. Vossen, Parton Fragmentation Functions, Prog. Part. Nucl. Phys. 91 (2016) 136–202. arXiv:1607.02521, doi:10.1016/j.pnpnp.2016.08.003.
- [8] A. Bianconi, S. Boffi, R. Jakob, M. Radici, Two hadron interference fragmentation functions. Part 2. A Model calculation, Phys. Rev. D62 (2000) 034009. arXiv:hep-ph/9907488, doi:10.1103/PhysRevD.62.034009.
- [9] R. L. Jaffe, X.-m. Jin, J. Tang, Interference fragmentation functions and the nucleon’s transversity, Phys. Rev. Lett. 80 (1998) 1166–1169. arXiv:hep-ph/9709322, doi:10.1103/PhysRevLett.80.1166.
- [10] D. Boer, R. Jakob, M. Radici, Interference fragmentation functions in electron positron annihilation, Phys. Rev. D67 (2003) 094003. arXiv:hep-ph/0302232, doi:10.1103/PhysRevD.67.094003.
- [11] Z.-B. Kang, A. Prokudin, P. Sun, F. Yuan, Extraction of Quark Transversity Distribution and Collins Fragmentation Functions with QCD Evolution, Phys. Rev. D93 (1) (2016) 014009. arXiv:1505.05589, doi:10.1103/PhysRevD.93.014009.
- [12] M. Radici, A. M. Ricci, A. Bacchetta, A. Mukherjee, Exploring universality of transversity in proton-proton collisions, Phys. Rev. D94 (3) (2016) 034012. arXiv:1604.06585, doi:10.1103/PhysRevD.94.034012.
- [13] A. Airapetian, et al., Single-spin asymmetries in semi-inclusive deep-inelastic scattering on a transversely polarized hydrogen target, Phys. Rev. Lett. 94 (2005) 012002. arXiv:hep-ex/0408013, doi:10.1103/PhysRevLett.94.012002.
- [14] A. Airapetian, et al., Evidence for a Transverse Single-Spin Asymmetry in Lepton production of $\pi^+\pi^-$ Pairs, JHEP 06 (2008) 017. arXiv:0803.2367, doi:10.1088/1126-6708/2008/06/017.
- [15] C. Adolph, et al., Transverse spin effects in hadron-pair production from semi-inclusive deep inelastic scattering, Phys. Lett. B713 (2012) 10–16. arXiv:1202.6150, doi:10.1016/j.physletb.2012.05.015.
- [16] M. G. Alekseev, et al., Measurement of the Collins and Sivers asymmetries on transversely polarised protons, Phys. Lett. B692 (2010) 240–246. arXiv:1005.5609, doi:10.1016/j.physletb.2010.08.001.
- [17] M. Alekseev, et al., Collins and Sivers asymmetries for pions and kaons in muon-deuteron DIS, Phys. Lett. B673 (2009) 127–135. arXiv:0802.2160, doi:10.1016/j.physletb.2009.01.060.
- [18] K. Abe, et al., Measurement of azimuthal asymmetries in inclusive production of hadron pairs in e^+e^- annihilation at Belle, Phys. Rev. Lett. 96 (2006) 232002. arXiv:hep-ex/0507063, doi:10.1103/PhysRevLett.96.232002.
- [19] A. Vossen, et al., Observation of transverse polarization asymmetries of charged pion pairs in e^+e^- annihilation near $\sqrt{s} = 10.58$ GeV, Phys. Rev. Lett. 107 (2011) 072004. arXiv:1104.2425, doi:10.1103/PhysRevLett.107.072004.
- [20] T. Bhattacharya, V. Cirigliano, S. Cohen, R. Gupta, H.-W. Lin, B. Yoon, Axial, Scalar and Tensor Charges of the Nucleon from $2+1+1$ -flavor Lattice QCD, Phys. Rev. D94 (5) (2016) 054508. arXiv:1606.07049, doi:10.1103/PhysRevD.94.054508.
- [21] J. R. Green, J. W. Negele, A. V. Pochinsky, S. N. Syritsyn, M. Engelhardt, S. Krieg, Nucleon Scalar and Tensor Charges from Lattice QCD with Light Wilson Quarks, Phys. Rev. D86 (2012) 114509. arXiv:1206.4527, doi:10.1103/PhysRevD.86.114509.
- [22] A. Abdel-Rehim, et al., Nucleon and pion structure with lattice QCD simulations at physical value of the pion mass, Phys. Rev. D92 (11) (2015) 114513, [Erratum: Phys. Rev.D93,no.3,039904(2016)]. arXiv:1507.04936, doi:10.1103/PhysRevD.92.114513, 10.1103/PhysRevD.93.039904.

- [23] Y. Aoki, T. Blum, H.-W. Lin, S. Ohta, S. Sasaki, R. Tweedie, J. Zanotti, T. Yamazaki, Nucleon isovector structure functions in (2+1)-flavor QCD with domain wall fermions, *Phys. Rev. D* **82** (2010) 014501. [arXiv:1003.3387](#), [doi:10.1103/PhysRevD.82.014501](#).
- [24] G. S. Bali, S. Collins, B. Glssle, M. Gckeler, J. Najjar, R. H. Rdl, A. Schfer, R. W. Schiel, W. Sldner, A. Sternbeck, Nucleon isovector couplings from $N_f = 2$ lattice QCD, *Phys. Rev. D* **91** (5) (2015) 054501. [arXiv:1412.7336](#), [doi:10.1103/PhysRevD.91.054501](#).
- [25] T. Bhattacharya, V. Cirigliano, S. D. Cohen, A. Filipuzzi, M. Gonzalez-Alonso, M. L. Graesser, R. Gupta, H.-W. Lin, Probing Novel Scalar and Tensor Interactions from (Ultra)Cold Neutrons to the LHC, *Phys. Rev. D* **85** (2012) 054512. [arXiv:1110.6448](#), [doi:10.1103/PhysRevD.85.054512](#).
- [26] D. Dubbers, M. G. Schmidt, The Neutron and Its Role in Cosmology and Particle Physics, *Rev. Mod. Phys.* **83** (2011) 1111–1171. [arXiv:1105.3694](#), [doi:10.1103/RevModPhys.83.1111](#).
- [27] V. Barone, A. Drago, P. G. Ratcliffe, Transverse polarisation of quarks in hadrons, *Phys. Rept.* **359** (2002) 1–168. [arXiv:hep-ph/0104283](#), [doi:10.1016/S0370-1573\(01\)00051-5](#).
- [28] L. Adamczyk, et al., Observation of Transverse Spin-Dependent Azimuthal Correlations of Charged Pion Pairs in $p^\uparrow + p$ at $\sqrt{s} = 200$ GeV, *Phys. Rev. Lett.* **115** (2015) 242501. [arXiv:1504.00415](#), [doi:10.1103/PhysRevLett.115.242501](#).
- [29] T. C. Rogers, P. J. Mulders, No Generalized TMD-Factorization in Hadro-Production of High Transverse Momentum Hadrons, *Phys. Rev. D* **81** (2010) 094006. [arXiv:1001.2977](#), [doi:10.1103/PhysRevD.81.094006](#).
- [30] L. Adamczyk, et al., Azimuthal transverse single-spin asymmetries of inclusive jets and charged pions within jets from polarized-proton collisions at $\sqrt{s} = 500$ GeV [arXiv:1708.07080](#).
- [31] Z.-B. Kang, X. Liu, F. Ringer, H. Xing, The transverse momentum distribution of hadrons within jets [arXiv:1705.08443](#).
- [32] Z.-B. Kang, A. Prokudin, F. Ringer, F. Yuan, Collins azimuthal asymmetries of hadron production inside jets [arXiv:1707.00913](#).
- [33] A. Adare, et al., Inclusive cross section and double-helicity asymmetry for π^0 production at midrapidity in $p+p$ collisions at $\sqrt{s} = 510$ GeV, *Phys. Rev. D* **93** (1) (2016) 011501. [arXiv:1510.02317](#), [doi:10.1103/PhysRevD.93.011501](#).
- [34] K. H. Ackermann, et al., STAR detector overview, *Nucl. Instrum. Meth. A* **499** (2003) 624–632. [doi:10.1016/S0168-9002\(02\)01960-5](#).
- [35] R. polarimeter group RHIC/CAD Physics Note 490.
- [36] M. Radici, Exploring universality of transversity in p-p collisions, *PoS QCDEV2016* (2017) 013. [arXiv:1611.03351](#).
- [37] A. Bacchetta, M. Radici, Dihadron interference fragmentation functions in proton-proton collisions, *Phys. Rev. D* **70** (2004) 094032. [arXiv:hep-ph/0409174](#), [doi:10.1103/PhysRevD.70.094032](#).
- [38] G. G. Ohlsen, P. W. Keaton, Techniques for measurement of spin-1/2 and spin-1 polarization analyzing tensors, *Nucl. Instrum. Meth.* **109** (1973) 41–59. [doi:10.1016/0029-554X\(73\)90450-3](#).
- [39] T. Sjostrand, S. Mrenna, P. Z. Skands, PYTHIA 6.4 Physics and Manual, *JHEP* **05** (2006) 026. [arXiv:hep-ph/0603175](#), [doi:10.1088/1126-6708/2006/05/026](#).
- [40] P. Z. Skands, Tuning Monte Carlo Generators: The Perugia Tunes, *Phys. Rev. D* **82** (2010) 074018. [arXiv:1005.3457](#), [doi:10.1103/PhysRevD.82.074018](#).
- [41] R. Brun, et al. User guide and reference manual.
- [42] H. H. Matevosyan, A. Kotzinian, A. W. Thomas, Studies of Azimuthal Modulations in Two Hadron Fragmentation of a Transversely Polarised Quark, *Phys. Lett. B* **731** (2014) 208–216. [arXiv:1312.4556](#), [doi:10.1016/j.physletb.2014.02.040](#).

Appendix A. Supplemental Material

η	A_{UT}	σ_{stat}	σ_{pid}	σ_{tb}	x	σ_x	z	σ_z	Q^2 (GeV ²)
-0.85	0.007	0.005	+0.001	-0.001	0.09	0.02	0.56	0.04	531
-0.57	0.003	0.004	+0.000	-0.000	0.07	0.02	0.61	0.04	447
-0.29	0.012	0.004	+0.002	-0.001	0.11	0.02	0.55	0.03	550
0.00	0.020	0.005	+0.003	-0.002	0.10	0.01	0.55	0.02	550
0.29	0.013	0.006	+0.002	-0.001	0.14	0.01	0.53	0.02	592
0.57	0.026	0.006	+0.004	-0.003	0.15	0.01	0.55	0.02	550
0.85	0.028	0.007	+0.004	-0.003	0.19	0.01	0.55	0.02	550

Table A.1: A_{UT} as a function of η corresponding to the top panel of Fig. 3 and x and z (bottom panel), where σ_{stat} is the statistical uncertainty, σ_{pid} is the particle identification systematic uncertainty, and σ_{tb} is the trigger bias systematic uncertainty. Q^2 corresponds with Fig. 1.

M_{inv} (GeV/ c^2)	p_T (GeV/ c)	η	A_{UT}	σ_{stat}	σ_{pid}	σ_{tb}
0.4	4.2	0.60	0.0041	0.0065	+0.0006	-0.0008
0.5	4.2	0.59	0.0057	0.0069	+0.0009	-0.0012
0.6	4.2	0.57	0.0055	0.0071	+0.0008	-0.0011
0.7	4.2	0.56	0.0045	0.0065	+0.0007	-0.0009
1.0	4.2	0.53	0.0073	0.0055	+0.0011	-0.0015
1.3	4.3	0.47	0.0126	0.0068	+0.0019	-0.0025
0.4	5.1	0.51	0.0047	0.0060	+0.0007	-0.0009
0.5	5.1	0.50	0.0009	0.0061	+0.0001	-0.0002
0.6	5.1	0.49	0.0140	0.0064	+0.0021	-0.0027
0.7	5.1	0.49	-0.0028	0.0057	+0.0004	-0.0005
0.9	5.1	0.47	0.0043	0.0049	+0.0007	-0.0008
1.3	5.1	0.44	0.0066	0.0061	+0.0010	-0.0013
1.7	5.2	0.41	0.0000	0.0113	+0.0000	-0.0000
0.4	6.3	0.49	0.0070	0.0063	+0.0010	-0.0013
0.5	6.3	0.49	0.0163	0.0062	+0.0024	-0.0029
0.6	6.3	0.48	0.0005	0.0064	+0.0001	-0.0001
0.7	6.3	0.48	0.0135	0.0057	+0.0020	-0.0024
0.9	6.3	0.46	0.0059	0.0049	+0.0009	-0.0011
1.3	6.3	0.44	-0.0086	0.0062	+0.0013	-0.0015
1.9	6.3	0.42	-0.0103	0.0081	+0.0015	-0.0019
0.4	8.0	0.48	-0.0038	0.0070	+0.0006	-0.0006
0.5	8.0	0.49	-0.0056	0.0065	+0.0008	0.0009
0.6	8.1	0.48	0.0107	0.0066	+0.0016	-0.0017
0.7	8.1	0.48	0.0055	0.0057	+0.0008	-0.0009
0.9	8.1	0.47	0.0204	0.0049	+0.0031	-0.0032
1.3	8.1	0.46	0.0068	0.0062	+0.0010	-0.0011
2.0	8.1	0.43	0.0039	0.0069	+0.0006	-0.0006
0.4	12.0	0.48	0.0023	0.0090	+0.0003	-0.0002
0.5	12.3	0.48	0.0269	0.0075	+0.0040	-0.0028
0.6	12.7	0.48	0.0207	0.0072	+0.0031	-0.0022
0.7	12.9	0.48	0.0249	0.0060	+0.0037	-0.0026
0.9	13.0	0.48	0.0298	0.0050	+0.0045	-0.0031
1.3	13.2	0.47	0.0196	0.0060	+0.0029	-0.0021
2.2	13.4	0.44	0.0104	0.0061	+0.0016	-0.0011

Table A.2: A_{UT} as a function of M_{inv} for $\eta > 0$ corresponding to Fig. 4, where σ_{stat} is the statistical uncertainty, σ_{pid} is the particle identification systematic uncertainty, and σ_{tb} is the trigger bias systematic uncertainty.

M_{inv} (GeV/ c^2)	p_T (GeV/ c)	η	A_{UT}	σ_{stat}	σ_{pid}	σ_{tb}
0.4	4.2	-0.60	0.0073	0.0065	+0.0011	-0.0015
0.5	4.2	-0.58	-0.0075	0.0069	+0.0011	-0.0015
0.6	4.2	-0.57	-0.0120	0.0071	+0.0018	-0.0024
0.7	4.2	-0.55	-0.0072	0.0065	+0.0011	-0.0015
1.0	4.2	-0.52	-0.0017	0.0054	+0.0003	-0.0004
1.3	4.3	-0.47	0.0015	0.0068	+0.0002	-0.0003
0.4	5.1	-0.51	0.0012	0.0059	+0.0002	-0.0002
0.5	5.1	-0.50	-0.0013	0.0061	+0.0002	-0.0002
0.6	5.1	-0.49	-0.0100	0.0064	+0.0015	-0.0019
0.7	5.1	-0.48	0.0034	0.0057	+0.0005	-0.0007
0.9	5.1	-0.47	0.0029	0.0049	+0.0004	-0.0006
1.3	5.1	-0.43	-0.0094	0.0061	+0.0014	-0.0018
1.7	5.2	-0.40	0.0146	0.0112	+0.0022	-0.0028
0.4	6.3	-0.49	0.0019	0.0063	+0.0003	-0.0003
0.5	6.3	-0.49	0.0069	0.0062	+0.0010	-0.0013
0.6	6.3	-0.48	0.0002	0.0065	+0.0000	-0.0000
0.7	6.3	-0.47	0.0058	0.0057	+0.0009	-0.0010
0.9	6.3	-0.46	0.0012	0.0049	+0.0002	-0.0002
1.3	6.3	-0.44	0.0051	0.0062	+0.0008	-0.0009
1.9	6.3	-0.41	-0.0103	0.0082	+0.0015	-0.0019
0.4	8.0	-0.48	0.0079	0.0070	+0.0012	-0.0013
0.5	8.0	-0.48	-0.0020	0.0064	+0.0003	-0.0003
0.6	8.1	-0.48	-0.0040	0.0066	+0.0006	-0.0006
0.7	8.1	-0.48	0.0105	0.0057	+0.0016	-0.0017
0.9	8.1	-0.47	0.0071	0.0049	+0.0011	-0.0011
1.3	8.1	-0.45	0.0007	0.0062	+0.0001	-0.0001
2.0	8.1	-0.43	0.0048	0.0069	+0.0007	-0.0008
0.4	12.0	-0.48	-0.0003	0.0090	+0.0000	-0.0000
0.5	12.3	-0.49	0.0106	0.0074	+0.0016	-0.0011
0.6	12.6	-0.48	0.0080	0.0072	+0.0012	-0.0008
0.7	12.9	-0.48	0.0025	0.0059	+0.0004	-0.0003
0.9	13.0	-0.47	0.0009	0.0048	+0.0001	-0.0001
1.3	13.2	-0.46	0.0060	0.0060	+0.0009	-0.0006
2.2	13.4	-0.44	-0.0007	0.0061	+0.0001	-0.0001

Table A.3: A_{UT} as a function of M_{inv} for $\eta < 0$, where σ_{stat} is the statistical uncertainty, σ_{pid} is the particle identification systematic uncertainty, and σ_{tb} is the trigger bias systematic uncertainty.

M_{inv} (GeV/ c^2)	p_T (GeV/ c)	η	A_{UT}	σ_{stat}	σ_{pid}	σ_{tb}
0.4	4.2	0.48	0.0019	0.0071	+0.0003	-0.0004
0.5	4.2	0.48	-0.0001	0.0087	+0.0000	-0.0000
0.6	4.2	0.48	-0.0082	0.0089	+0.0012	-0.0017
0.7	4.2	0.48	0.0058	0.0086	+0.0009	-0.0012
1.0	4.2	0.47	-0.0222	0.0068	+0.0033	-0.0045
1.3	4.3	0.46	-0.0078	0.0078	+0.0012	-0.0016
0.4	5.1	0.48	-0.0028	0.0066	+0.0004	-0.0005
0.5	5.1	0.48	-0.0046	0.0079	+0.0007	-0.0009
0.6	5.1	0.48	0.0031	0.0081	+0.0005	-0.0006
0.7	5.1	0.48	0.0003	0.0078	+0.0000	-0.0001
0.9	5.1	0.47	-0.0058	0.0063	+0.0009	-0.0011
1.3	5.1	0.46	-0.0023	0.0072	+0.0004	-0.0004
1.7	5.2	0.44	0.0027	0.0126	+0.0004	-0.0005
0.4	6.3	0.48	0.0073	0.0071	+0.0011	-0.0013
0.5	6.3	0.48	0.0061	0.0081	+0.0009	-0.0011
0.6	6.3	0.48	0.0105	0.0083	+0.0016	-0.0019
0.7	6.3	0.48	0.0138	0.0080	+0.0021	-0.0025
0.9	6.3	0.47	-0.0021	0.0065	+0.0003	-0.0004
1.3	6.3	0.46	-0.0054	0.0076	+0.0008	-0.0010
1.9	6.3	0.44	-0.0017	0.0092	+0.0003	-0.0003
0.4	8.0	0.48	0.0153	0.0081	+0.0023	-0.0024
0.5	8.0	0.48	0.0011	0.0086	+0.0002	-0.0002
0.6	8.0	0.48	0.0119	0.0087	+0.0018	-0.0019
0.7	8.1	0.48	-0.0046	0.0083	+0.0007	-0.0007
0.9	8.1	0.47	0.0040	0.0066	+0.0006	-0.0006
1.3	8.1	0.46	0.0091	0.0080	+0.0014	-0.0014
2.0	8.1	0.44	-0.0086	0.0081	+0.0013	-0.0014
0.4	11.7	0.48	0.0317	0.0110	+0.0048	-0.0033
0.5	12.4	0.48	-0.0101	0.0098	+0.0015	-0.0011
0.6	12.6	0.48	0.0089	0.0097	+0.0013	-0.0009
0.7	12.7	0.48	0.0070	0.0091	+0.0010	-0.0007
0.9	12.9	0.47	0.0143	0.0071	+0.0021	-0.0015
1.3	13.0	0.46	-0.0010	0.0083	+0.0001	-0.0001
2.2	13.2	0.44	0.0051	0.0076	+0.0008	-0.0005

Table A.4: A_{UT} for same-charge, momentum-ordered pion pairs as a function of M_{inv} for $\eta > 0$ corresponding to Fig. 5, where σ_{stat} is the statistical uncertainty, σ_{pid} is the particle identification systematic uncertainty, and σ_{tb} is the trigger bias systematic uncertainty.

M_{inv} (GeV/ c^2)	p_T (GeV/ c)	η	A_{UT}	σ_{stat}	σ_{pid}	σ_{tb}
0.4	4.2	-0.48	0.0007	0.0071	+0.0001	-0.0001
0.5	4.2	-0.48	-0.0018	0.0087	+0.0003	-0.0004
0.6	4.2	-0.48	0.0081	0.0090	+0.0012	-0.0016
0.7	4.2	-0.48	0.0108	0.0086	+0.0016	-0.0022
1.0	4.2	-0.47	0.0131	0.0068	+0.0020	-0.0026
1.3	4.3	-0.46	-0.0035	0.0078	+0.0005	-0.0007
0.4	5.1	-0.48	0.0098	0.0066	+0.0015	-0.0019
0.5	5.1	-0.48	-0.0029	0.0079	+0.0004	-0.0006
0.6	5.1	-0.48	0.0036	0.0081	+0.0005	-0.0007
0.7	5.1	-0.48	-0.0103	0.0078	+0.0015	-0.0020
0.9	5.1	-0.47	0.0047	0.0063	+0.0007	-0.0009
1.3	5.1	-0.46	-0.0097	0.0072	+0.0015	-0.0019
1.7	5.2	-0.44	-0.0316	0.0126	+0.0047	-0.0060
0.4	6.3	-0.48	-0.0012	0.0071	+0.0002	-0.0002
0.5	6.3	-0.48	-0.0046	0.0081	+0.0007	-0.0008
0.6	6.3	-0.48	-0.0001	0.0083	+0.0000	-0.0000
0.7	6.3	-0.48	0.0044	0.0080	+0.0007	-0.0008
0.9	6.3	-0.47	0.0032	0.0065	+0.0005	-0.0006
1.3	6.3	-0.46	0.0050	0.0076	+0.0007	-0.0009
1.9	6.3	-0.44	-0.0016	0.0092	+0.0002	-0.0003
0.4	8.0	-0.48	0.0051	0.0081	+0.0008	-0.0008
0.5	8.0	-0.48	-0.0073	0.0085	+0.0011	-0.0012
0.6	8.0	-0.48	0.0119	0.0087	+0.0018	-0.0019
0.7	8.0	-0.48	-0.0072	0.0083	+0.0011	-0.0011
0.9	8.1	-0.47	0.0047	0.0067	+0.0007	-0.0007
1.3	8.1	-0.46	-0.0097	0.0080	+0.0015	-0.0015
2.0	8.1	-0.44	0.0057	0.0081	+0.0009	-0.0009
0.4	11.8	-0.48	0.0100	0.0110	+0.0015	-0.0011
0.5	12.4	-0.48	-0.0112	0.0098	+0.0017	-0.0012
0.6	12.6	-0.48	0.0020	0.0097	+0.0003	-0.0002
0.7	12.7	-0.48	0.0167	0.0091	+0.0025	-0.0018
0.9	12.8	-0.47	0.0016	0.0071	+0.0002	-0.0002
1.3	13.0	-0.46	0.0026	0.0083	+0.0004	-0.0003
2.2	13.1	-0.44	0.0113	0.0076	+0.0017	-0.0012

Table A.5: A_{UT} for same-charge, momentum-ordered pion pairs as a function of M_{inv} for $\eta < 0$ corresponding to Fig. 5, where σ_{stat} is the statistical uncertainty, σ_{pid} is the particle identification systematic uncertainty, and σ_{tb} is the trigger bias systematic uncertainty.